(Article begins on next page)

Cryogenic 2-13 GHz Eleven Feed for Reflector Antennas in Future Wideband Radio Telescopes

Jian Yang, *Senior Member, IEEE*, Miroslav Pantaleev, Per-Simon Kildal, *Fellow, IEEE*, Benjamin Klein, Yogesh Karandikar, Leif Helldner, Niklas Wadefalk, Christopher Beaudoin

***Abstract*—The system design of a cryogenic 2-13 GHz feed is considered with emphasis on its application in future wideband radio telescope systems. The feed is based on the so-called Eleven antenna and the design requires careful integration of various sub-designs in order to realize cryogenic operation. The various sub-designs include the electrical design of the Eleven antenna, design of the critical center puck, alternative solutions for integrating the Eleven antenna with low noise amplifiers (LNAs), mechanical and cryogenic design and tests, and system noise temperature estimation and measurements. A great deal of simulated and measured results are presented throughout this paper, including the electrical, mechanical and cryogenic performance, and an assessment of the system noise temperature. The objective of this work is to present a good feed candidate that is well-suited for VLBI2010 and SKA radio telescopes. Further developments needed to completely fulfill the requirements for these future wideband radio telescopes are also discussed.**

***Index Terms*—radio telescope, reflector antenna, the Eleven feed, wideband feed, cryogenic technology.**

I. Introduction

THE future development of radio astronomy requires large decade-bandwidth telescopes, such as 1-10 GHz proposed for the mid frequency dish array of the SKA (Square Kilometer Array) [1] and 2-14 GHz for VLBI2010 (Very Long Baseline Interferometry 2010) [2]. These frequency bands are quite similar to the FCC regulated Ultra-wideband (UWB) 3.1-10.6 GHz for future short-range communications and radars [3]. However, the requirements imposed on the radiation performance of decade-bandwidth antennas needed to feed future radio telescopes are much stricter than those of UWB communication applications, so the former antennas will have to be much more complex. Additionally, decade-bandwidth radio telescopes must have an extremely low system noise temperature (about 35 K), which is not the case in other UWB applications.

VLBI2010 and mid frequency SKA radio telescopes will be realized by single-beam reflector antennas. In the latter case, approximately 1,200 dishes of $15m$ diameter are needed, and a system noise temperature of about 35 K is required in order to reach a figure of merit, A/T (see definition in Section VI), of $5000m^2/K$ [4] (corresponding to an A/T per square meter physical aperture size of $0.02m^2/K$). Achievement of such sensitivity is a primary goal of this work. Therefore, cryogenically-cooled LNAs are critical for both VLBI2010 and mid-frequency SKA systems. It is also important that the feed and its cryogenic chamber (cryostat) be sufficiently compact in order to avoid additional blockage by these components. Consequently, size and cryogenic cooling concerns (such as out-gassing and thermally-induced mechanical stress) play important roles in the design of decade-bandwidth feeds for VLBI2010 and SKA radio telescopes.

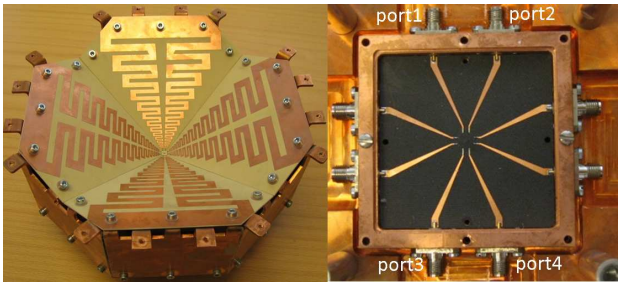

Fig. 1. Photo of the manufactured Eleven feed, and the descrambling board at the rear side of the ground plane (amplified, not in scale).

The Eleven antenna is a decade-bandwidth log-periodic dual-dipole array, developed at Chalmers University of Technology (Chalmers) since 2005 [4]-[8]. Its properties as a feed for reflector antennas have been demonstrated for radio telescope applications - such as a nearly constant beamwidth with about 11 dBi directivity, a fixed phase center location (over the entire decade bandwidth), and low profile and simple geometry. This paper is intended to present the latest developments of a cryogenically-coolable Eleven feed system for VLBI2010 and SKA, shown in Fig. 1, which includes the integration and co-design with cryogenic low noise amplifiers (LNAs).

The Eleven antenna was originally proposed by P.-S. Kildal and presented in [5], and two hardware realizations, operating below 2 GHz, are described in [6] and [7]. The first successful attempt to make a high frequency model working up to 10 GHz is described in [8], but it suffered from some mechanical and cryogenic problems. These problems have been solved with the model described in this paper, being functional up to 13 GHz. In addition to applications in radio telescopes, the Eleven antenna can be applied to other areas, e.g., to produce the

Manuscript submitted December 31, 2009.

J. Yang (e-mail: jian.yang@chalmers.se) and P.-S. Kildal are with the Department of Signals and Systems, Y. Karandikar and N. Wadefalk with Department of Microtechnology and Nanoscience, Miroslav Pantaleev and Leif Helldner are with Onsala Space Observatory, all at Chalmers University of Technology, S-41296 Gothenburg, Sweden. Benjamin Klein is with Harte-beeshoek Radio Astronomy Observatory, South Africa. Christopher Beaudoin is with MIT Haystack Observatory, Westford, MA 01886-1299, USA.

This work was supported in part by Swedish Foundation for Strategic Research (SSF) via the CHARMANT antenna systems research center at Chalmers.

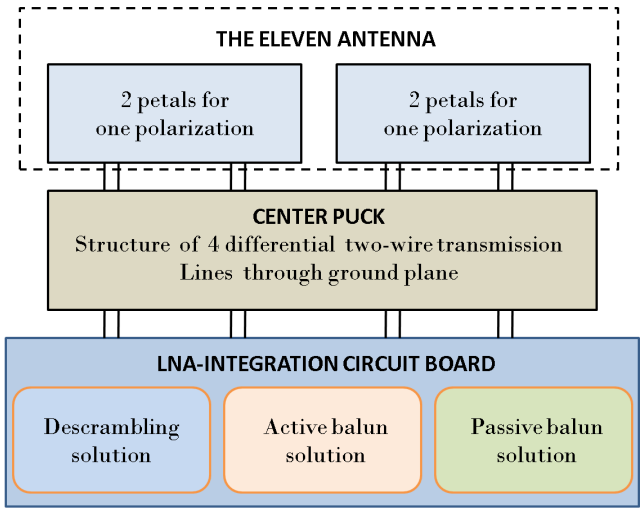

Fig. 2. System configuration of the Eleven feed.

radiation patterns with nulls on axis required for mono-pulse tracking in e.g. satellite communication terminals [9], and as monitoring antennas in satellite communication systems. In such applications it may also be advantageous to combine the Eleven antenna, with a centrally located high frequency horn, in order to reach Ka-band, see [10].

Different from the previous publications about the Eleven antenna, this paper presents the system design of a complete cryogenic 2-13 GHz Eleven feed system. Firstly, this effort involved the electrical design of log-periodic radiating dipole petals etched on a thin stiff dielectric substrate. This substrate is used for mechanical support; previous petal designs were entirely metal and could not be used in designs above 3 GHz. Secondly, a transition from dipoles to microstrip lines (henceforth referred to as the center puck) was designed to couple the four radiating dipole arrays on the front side of the ground plane to a descrambling board on the rear side. Also discussed in this paper are alternative integration methods for antenna and low-noise-amplifiers (LNAs), mechanical and cryogenic design and tests, and system noise temperature estimation and measurements.

The main focus of this paper is to provide a high level description of the various designs, tests, and simulations performed to achieve optimal system performance. As such, references are cited for the detailed description of each component comprising the system integration. In this way, the interested reader may obtain more detailed information, on each system integration component.

The paper is organized as follows. In Section II, the system configuration is described. In Section III, the four log-periodic dipole arrays (petals) is presented along with the description of the electric design, the definitions of different Eleven feed models, the room and cryogenic temperature performance. In Section IV, the descrambling and LNA-integration alternatives are discusses in detail, including the single-ended 8 port solution with center puck, the active balun solution, the passive balun solution, and the packaging using lid of nails. In Section V, we focus on mechanical and cryogenic design and testing. In Section VI, the figure of merit and the system noise temperature of the Eleven antenna system are analyzed with the measured and estimated Tsys for feed pointing towards zenith and estimated A/T of the feed in reflectors.

It should be mentioned that there are also other feed candidates for VLBI2010 and SKA radio telescopes, such as the quadridge horn [11] and the quasi self-complementary antenna [12]. The main drawback of the quadridge horn as a feed for reflectors is that its beamwidth and phase center location vary with frequency, which leads to a low aperture efficiency; see the comparison of the radiation performance between the Eleven antenna and the quadridge horn in [13]. The quasi self-complementary antenna [12] is also a log-periodic dual-dipole-like antenna, but it has a polarization that squints with frequency and no hardware has yet been realized above 4 GHz. The recent ultra wideband antenna in [14] is wideband, but it is too large in terms of wavelengths to be used as a reflector feed at SKA and VLBI2010 frequencies.

II. System Configuration

The configuration of the complete Eleven feed receiving antenna system is represented by the block diagram in Fig. 2, with reference to the already mentioned photo in Fig. 1. It consists of three parts: the four log-periodic dipole petals (i.e., the Eleven antenna), the center puck (combining the front and rear sides of the ground plane), and the rear-side circuit board (for integration of the LNAs and descrambling of the four balanced ports of the log-periodic dipoles).

The Eleven feed can receive dual linearly polarized waves, and, thus dual circular polarization reception is, of course, also available by linear quadrature combination of the two orthogonal linearly polarized ports, either by hardware, or by software after detection. The antenna, for each linear polarization, consists of two oppositely-located log-periodic dipole arrays, i.e. two dipole petals. In the center of the geometry each dipole petal is connected to a balanced twin-lead transmission line, with a characteristic impedance of 200 ohms. The two twin-lead transmission lines of oppositely-located petals must be combined with the same amplitudes and phases in order to receive one linear polarization. Similarly, the two opposing twin-lead lines, of the two remaining oppositely-located petals, must be combined to receive the orthogonal linear polarization.

The center puck consists of three sub-parts: first, an inner support structure for the four dipole petals at the front side of the ground plane; second, the four twin-lead transmission lines that connect the antenna petals on the front side of the ground plane to the descrambling LNA-integration circuit board on the rear side of the ground plane; and third, a shielding and packaging structure for the four twin-lead lines and the descrambling board with LNAs.

For the descrambling and LNA-integration circuit board, three alternative solutions are proposed: an 8-port solution, an active balun solution, or a passive balun solution. The main reason for having three such circuit board solutions is to provide flexibility to achieve the most cost-effective

solution for different scenarios (e.g. for antenna testing, and adoption to the availability of single-ended or differential LNA alternatives).

In the 8-port circuit board solution shown in Fig. 2, the four balanced twin-lead ports are transformed to eight single-ended coaxial ports. This enables testing of the Eleven antenna before being integrated with the LNAs, in order to assess the performance of the antenna itself. Additionally, the 8-port solution offers more functions, such as, tracking performance by properly combining ports to generate so-called mono-pulse type "difference" patterns with nulls in the main beam direction of the normal "sum" pattern [9], and it can be used in diversity and MIMO systems [15].

Each of the four log-periodic dipole petals can be fed using a balun which is a hardware component, or circuit, that transforms the balanced twin-lead feed line of the dipole to an unbalanced single-ended line, without exciting common modes. A common mode corresponds to the excitation of equal voltages on the two dipole arms with respect to the ground, and significantly degrades the normal dipole radiation pattern. The active balun solution in Fig. 2 utilizes four wideband differential LNAs, leading to a very compact integrated solution. Differential LNAs have balanced input ports and single-ended outputs. In the passive balun solution in Fig. 2, four wideband passive baluns and two wideband power combiners are used so that the Eleven feed can be integrated with two single-ended LNAs, one per linear polarization. The pros and cons of these three alternatives are discussed in Section IV.

III. The Four Log-periodic Dipole Arrays (Petals)

The basic geometry of the Eleven antenna is two parallel folded dipoles, separated by half a wavelength and located above a ground plane. Then, the pair of folded dipoles is extended with a log-periodic scaling factor to a number of pairs and the corresponding folded dipoles of each pair are cascaded one after another, to form two opposing log-periodic dipole arrays, which are referred to as petals here. The dual polarized Eleven antenna has four equal petals, as shown in Fig. 1. The radiation field function of the Eleven feed is determined by the geometry of the four petals which also has a strong impact on the input reflection coefficient.

A. Electrical Design

The goal of the electric design of the present Eleven antenna is to minimize the reflection coefficient at the input port of the petals, and at the same time to retain a good radiation performance, between 2 and 13 GHz. By avoiding a strong reflection at the input port of the feed, the system noise temperature is optimized as discussed in Section VI.

Analytic or quasi-analytic analysis of the radiation field function of the Eleven antenna is only available for the basic geometry, i.e. for one pair of folded dipoles [16] over an infinite ground plane, which provides the optimum ranges of the dimensions of each radiating dipole pair for the best radiation pattern shapes. Analytic models for the impedance of a single radiating folded dipole pair is available in [17], which gives an insight into how the Eleven antenna works, and in particular why the folded dipole is preferred over a normal dipole with single-wire arms. However, analytical impedance model for multiple cascaded folded dipoles is not yet available. Therefore, the optimum dipole petal geometries for low input reflection coefficient must be determined by numerical analysis, using a general electromagnetic solver. Unfortunately, this is very time consuming, as the size of the whole log-periodic dipole petal geometry is very large in terms of wavelengths at the highest frequency. Numerical optimization becomes almost impossible unless the log-periodic variation is accounted for in some way, to reduce computation time. Therefore, a special computational approach for log-periodic geometries was developed [18], referred to as the partial array method.

The above-mentioned partial array method can be used to predict the reflection coefficient of a complete large log-periodic array (with a large number of elements) from the S parameters of a sub-component of the log-periodic pattern as described in detail in [18]. With this technique, the computation time is considerably reduced, and thereby allows for extensive optimizations. In the present design we applied the partial array method and genetic algorithm to optimize the dimensions of the dipole petals, which provides the lowest reflection coefficient for a linearly polarized Eleven antenna. This means that we analyze only two opposing dipole petals, with both being correctly excited (equal amplitude and phase), and we choose the allowed dimensions within ranges that give the best radiation field functions. The radiation performance of the feed is judged by the values of the feed efficiency, i.e. the aperture efficiency of blockage-free prime focus reflector with certain subtended angle, as seen from the focal point. The resulting reflection coefficient of the optimized linearly-polarized Eleven antenna, as simulated by CST Microwave Studio [19], is below -9.4 dB over 2 - 13 GHz - when referred to an input balanced port impedance of 200 ohm [18] on both dipole petals. This 200 ohm balanced input port impedance appears to be intrinsic to the Eleven antenna. The complete dual polarized 2-13 GHz Eleven antenna which includes 14 purely log-periodic dipoles per petal, is obtained by adding two more dipole petals, located in the orthogonal azimuth plane relative to the first two petals, and otherwise being identical to them. For details, please refer to [18]. It is worth pointing out here that the innermost shortest dipole, resonates at 17.3 GHz, and the outermost longest dipole at 1 GHz, which means that the frequency span between the longest and the shortest dipoles is much larger than the operating frequency band of the array.

B. Definitions of Different Eleven Feed Models

We refer to the above numerically optimized dual-polarized model of the Eleven antenna as the "design model". From initial simulations and measurements of the design model, it was found that at the higher end of the frequency band, the input reflection coefficient degraded to -6 dB when the orthogonal dipole petals and the center puck is included. Therefore, we performed a small manual tuning of the dimensions of the design model with the help of simulations, which resulted in

reflection coefficient below -10 dB over the whole frequency band (2 - 14 GHz). We refer to this model as the "tuned design model". Four 2 - 14 GHz Eleven feeds based on the present design model have been manufactured, and they have been tested at various laboratories. The first was ordered by Norwegian Mapping Authority "Statkart" [20] and is therefore referred to as the Statkart model. This had dimensions that were identical to those of the design model. The remaining three models were tuned design models: one (the second) ordered by and delivered to Vertex Antennentechnik GmbH [21] referred to as the Vertex model, a third cryogenic testing model intended for cryogenic testing at Chalmers, and a forth spare model. There are some minor mechanical differences between the different models, and therefore we refer to them by different names for quality control.

C. Room Temperature Performance

All simulated and measured results shown in this section are for the full dual polarized geometry of the Eleven feed, including four antenna petals, the center puck, and the 8-port circuit board, all shown in Fig. 1. SMA coaxial connectors are used at all eight circuit board ports.

Fig. 3 shows the simulated and measured reflection coefficients of the Statkart and Vertex models. The Statkart model was measured at Caltech (California Institute of Technology) [22], and the Vertex model at OSO (Onsala Space Observatory) [23], both by using a 4-port VNA (vector network analyzer). The plotted reflection coefficient Γ is obtained from the measured 4-port S parameters of the feed by using [9]

$$\Gamma = S_{11} - S_{12} + S_{13} - S_{14}. \quad (1)$$

which corresponds to using an ideal feeding network consisting of two ideal 180° hybrids (baluns) and one ideal 3-dB power combiner, as shown in Fig. 3(c). The simulated results are, for both models, obtained by using CST Microwave Studio on the complete geometry of the model - including center puck and rear 8-port circuit board. It is observed that the reflection coefficients of the Statkart model, in Fig. 3(a), are below -10 dB at most frequency points between 2 and 10 GHz, whereas it degrades to -6 dB between 10 and 14 GHz. Fig. 3(b) shows that the measured reflection coefficients of the Vertex model are below -10 dB over the whole band for both polarizations. The agreements between the simulated and measured results are quite good in both cases, even though the detailed behavior of the two reflection coefficients deviate below -10 dB. The reflection coefficient of the present Eleven feed has therefore been improved by 2 dB below 10 GHz and up to 6 dB above 10 GHz compared to the previous Eleven feed documented in [8].

Note that the mechanical tolerances have some impact on the reflection coefficient performance of the feed, which can be seen from the difference between the reflection coefficients of the two polarizations in Fig. 3(b). Simulations using CST Microwave Studio shows that a 0.05 mm manufacturing error in the width of the first folded dipoles has significant effect on the reflection coefficient at high frequencies. Therefore, we will try to improve the manufacture tolerances on future models.

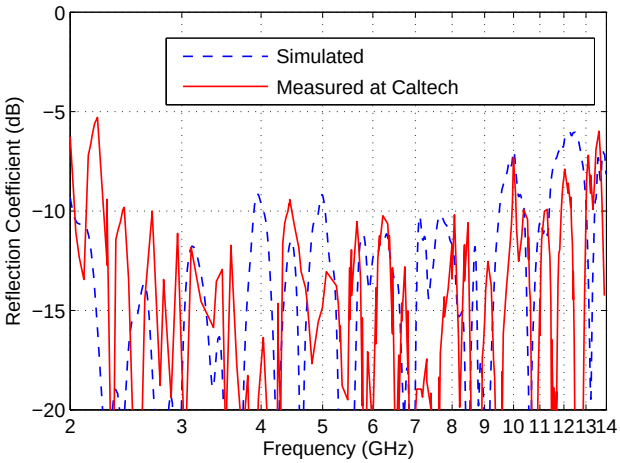

(a) Statkart model

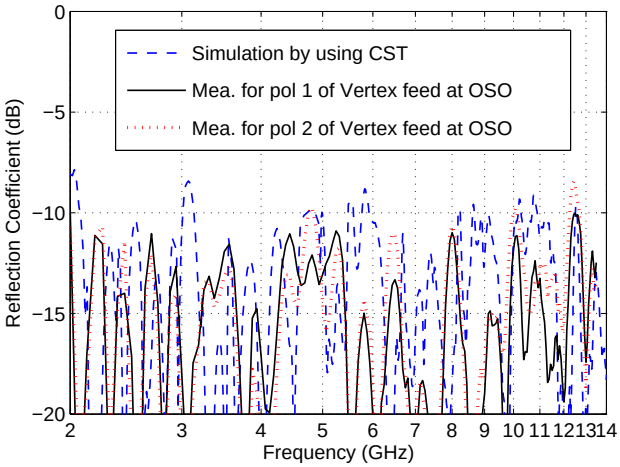

(b) Vertex model

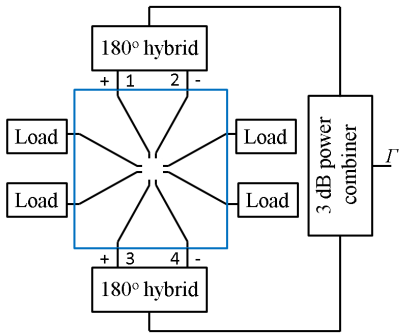

(c) Ideal feeding network

Fig. 3. Simulated and measured reflection coefficients of the a) Statkart and b) Vertex models of the Eleven feed. The results corresponds to what can be observed on the power-combined port of c) the ideal feed network.

The Eleven antenna satisfies the condition for constant radiation characteristics of a log-periodic array, as stated in [24], except for the thin dielectric substrate that is not scaled log-periodically and therefore will cause some degradation at high frequencies. This is reduced, to some degree, by milling the substrate down, as much as possible, in the central region.

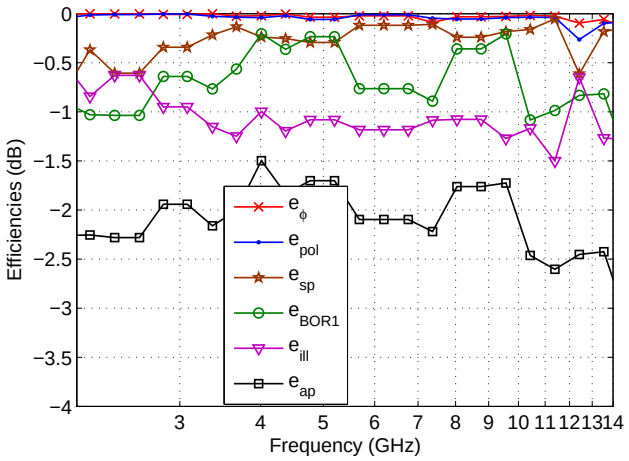

(a) From computed far field functions

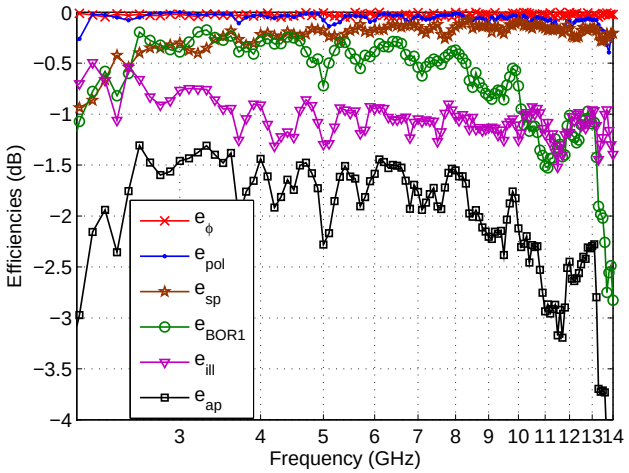

(b) From measured far field functions

Fig. 4. Aperture efficiency and its subefficiencies when the Vertex model illuminates a paraboloid. Center blockage is neglected. Results are based on a) computed and b) measured complex far fields.

Therefore, good performance over the whole 2 - 14 GHz bandwidth is expected except for some degradation at the high frequencies.

The complex far-field functions $G_\theta(\theta, \varphi)$ and $G_\varphi(\theta, \varphi)$ of the Eleven feed were measured in the spherical near-field test range at DTU (Technical University of Denmark). The angular range covered 0° to 180° for the polar θ value and 0° to 360° for the azimuth φ value, both with intervals of 1°, where the polar and azimuth angles are defined in a coordinate system with z-axis located vertically to the ground plane and at the central point between all dipole petals. Three models were measured (the Vertex model, the cryogenic test model and the spare model), and we could not see any significant differences between the results. Thus the radiation field of the Eleven feed is less sensitive to mechanical tolerances than the reflection coefficient is. Therefore, we present the radiation patterns and efficiencies only for one model in this paper (the Vertex model).

Fig. 4 shows the total aperture efficiency and its subefficiencies, as defined in [25] and [26], when the feed illuminates a symmetrical paraboloid in which center blockage loss is neglected. The efficiencies are computed both from simulated radiation field functions (Fig. 4(a)) and measured ones (Fig. 4(b)). In both cases the paraboloid has a subtended half angle of 60 $\circ$, corresponding to an $F/D = 0.433$. The subefficiencies are discussed below.

The radiation field patterns are plotted in Fig. 5. The BOR_1 radiation patterns in Fig. 5(b) are obtained by removing all φ-terms of higher order than order $n = 1$ from the total radiation field function, as defined in [26]. These higher order terms result in a power loss in the BOR_1 efficiency.

The BOR_1 efficiency e_{BOR1} is the ratio of power in the $n = 1$ terms of the Fourier φ-series of the far field function of the antenna to the total power radiated by the antenna. It is well known that only the $n = 1$ term contributes to the axial radiation field (i.e. gain) of a rotationally symmetric reflector antenna, and that the higher order φ terms represent a power loss to the sidelobes [26][27]. From Fig. 4, it can be observed that the BOR_1 efficiency is higher than -1dB from 2.5 to 10 GHz, higher than -1.5 dB in the ranges 2-2.5 GHz and 10 - 13 GHz, but drops to -3 dB at 14 GHz. Therefore, from 2.0 to 13 GHz, the BOR_1 efficiency is good.

A study is currently being carried out to solve the problem of the reduction of the BOR_1 efficiency above 10 GHz. Some preliminary results indicate that the reason is surface waves in the dielectric support of the dipole petals, and that these surface waves are excited at the point where the vertical twin-lead lines through the ground plane, are connected to the dipole petals [28].

The polarization efficiency, representing power lost to cross-polar sidelobes, is high ($e_{pol} > -0.2$ dB), as well as the phase efficiency ($e_\phi > -0.1$ dB). The latter represents the gain reduction due to phase errors over the reflector aperture. The high phase efficiency is achieved because the phase center of the Eleven antenna is located almost exactly at the ground plane, over the whole frequency band. The phase efficiency is computed for the case when the feed is located in such way that the focal point of the paraboloid coincides with the center of the ground plane. The illumination efficiency e_{ill} is about -1 dB at all frequencies. The frequency variations of e_{ill} are small due to the almost constant beamwidth of the radiation pattern over the whole frequency band 2 - 13 GHz. This is seen in Fig. 5 which shows the measured co- and cross-polar radiation patterns and their BOR_1 components in the $\varphi = 45^\circ$ plane.

The constant beamwidth feature leads also a high spillover efficiency e_{sp} over the whole band. It should be emphasized here that the constant beamwidth and the constant phase center location over a decade bandwidth or more are two unique features of the Eleven antenna, which has not been found in other UWB antennas. Therefore, the total aperture efficiency is also high, i.e. higher than -3 dB (50%) over 2 - 13 GHz.

The simulated and measured directivities over 2 - 14 GHz are shown in Fig. 6. The agreement between the simulated and measured values is within 1.5 dB between 2.3 and 14 GHz, which is good, in particular because the variations with frequency are very similar except below 2.3 GHz. The

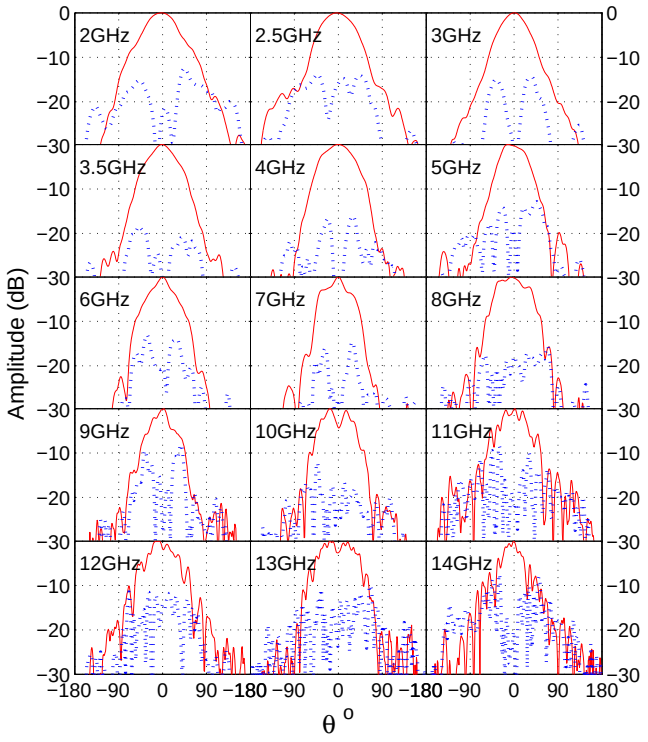

(a)

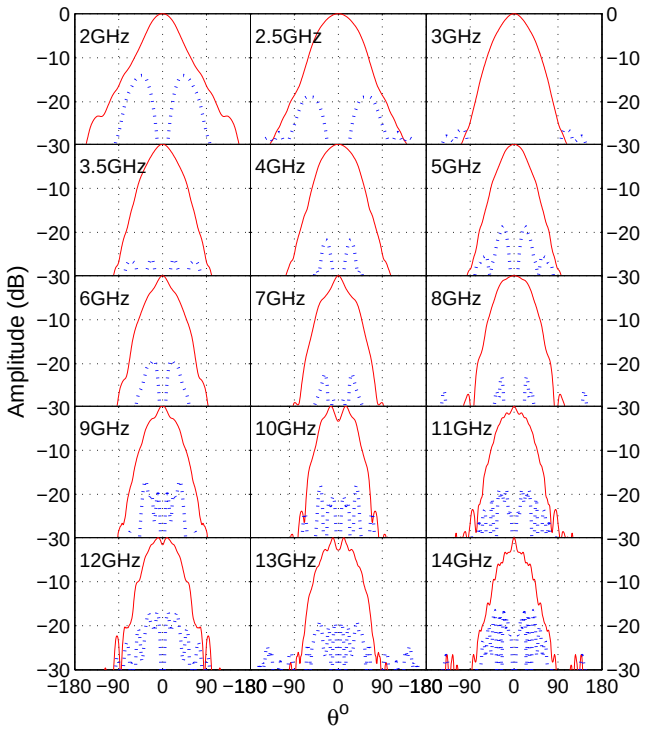

(b)

Fig. 5. Measured co(solid)- and cross(dashed)-polar radiation patterns at 15 frequencies in $\varphi = 45°$ plane of the Vertex model. The upper graph shows the patterns of the total radiation field, and the lower graph of the BOR_1 components of the field.

difference at low frequency is probably due to the fact that the surrounding mechanical support structure of the dipole petals was not modeled in detail in the far field computations.

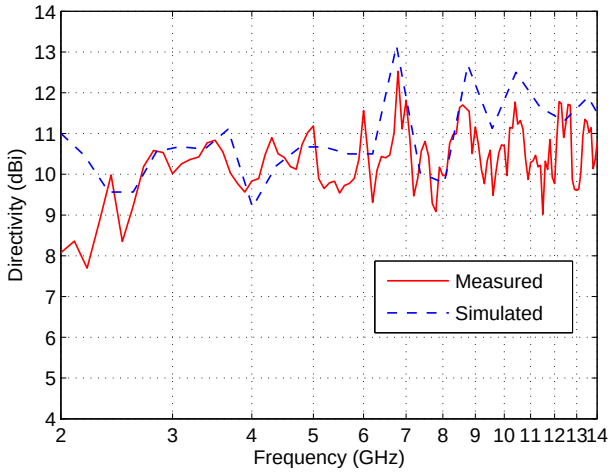

Fig. 6. Computed and measured directivities of the Vertex model.

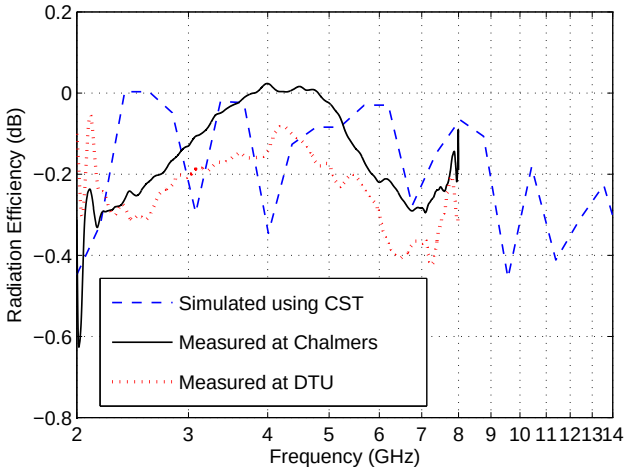

Fig. 7. Radiation efficiency of the cryogenic test model of the Eleven feed measured both in the spherical near-field test range at DTU and in the reverberation chamber at Chalmers, and computed using CST Microwave Studio.

It is also critical for feeds used in radio telescopes to have high radiation efficiency e_{rad}, which measures the ohmic losses of an antenna. The total radiation efficiency $e_{tot.rad}$ is the radiation efficiency multiplied with the mismatch factor, i.e. $e_{tot.rad} = e_{rad}(1 - |\Gamma|^2)$. Both e_{rad} and $e_{tot.rad}$ of the Eleven feed have been measured over 2 - 8 GHz by two methods: the spherical near-field method at DTU and the reverberation chamber method at Chalmers [29]. The reason for the measured frequency range of only 2 - 8 GHz is the present limitations of both methods above 8 GHz. However, we have computed the radiation efficiency over the whole frequency range by numerical simulations in CST Microwave Studio. Fig. 7 shows the measured and computed data. From the figure, it is concluded that the radiation efficiency (ohmic loss) of the Eleven feed is between -0.1 dB and -0.4 dB over

2 - 8 GHz, and we believe that the radiation efficiency is between -0.4 and -0.5 dB up to 14 GHz. The reason that the radiation efficiency of the Eleven antenna does not degrade with increasing frequency is that the path length between the LNAs and the radiating folded dipoles is much shorter at high frequency than at low frequencies.

D. Cryogenic Performance

A very important aspect in design of a cryogenic feed is to assess the performance of the feed when it is cooled down to cryogenic temperature. Fig. 8 shows the simulated geometrical deformation of the Eleven feed when it is cooled down to 20 K, by using the software ANSYS [30]. From the simulation, it can be observed that the maximum deformation of the petals is about 0.3mm at the outer part of the petals, and 0.1 mm at the center.

The Eleven feed with integrated LNAs was housed in a test cryostat, as shown in Fig. 9 and described in Section V. Reflection coefficient of the cryogenic test model of the Eleven feed was measured with the feed located inside this cryostat under cryogenic conditions. Three measured cases are compared in Fig. 10: the feed located outside the cryostat at room temperature, the feed inside the cryostat at room temperature, and the feed inside the cryostat at a cryogenic temperature of 48 K. From the measured data it can be concluded that the impedance matching of the Eleven feed is mostly unaffected by the cryostat walls surrounding the feed and the cryogenic temperatures.

At present we cannot directly measure the radiation performance at cryogenic temperature due to limited resources. However, from our experience, the radiation performance is less sensitive to small deformations than the reflection coefficient is. The measured reflection coefficients in Fig. 10 therefore can be used as an indicator that the radiation performance will not change much when the feed is at cryogenic temperature. Some numerical studies of the effect of the cryostat walls and window on the radiation pattern have been done, and they do not indicate any problems either. The reason for the minor influence of the cryostat is that the three outer dipoles of the Eleven feed structure that are closest to the wall of the cryostat do not radiate above 2 GHz. They are only used to properly terminate the log-periodic structure so that the radiation impedance is the same over the whole operational frequency band 2-13 GHz.

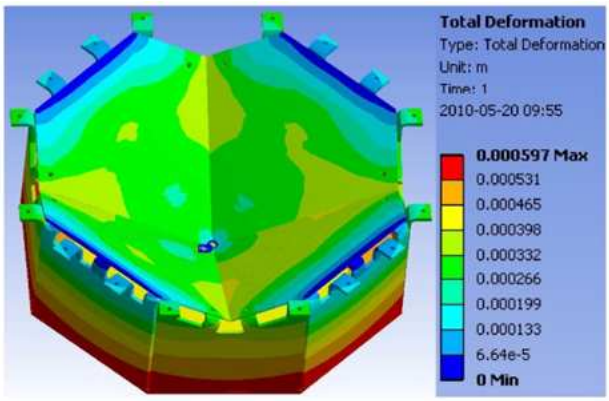

Fig. 8. Simulated geometrical deformations of the Eleven feed when it is at the cryogenic temperature of 20 K.

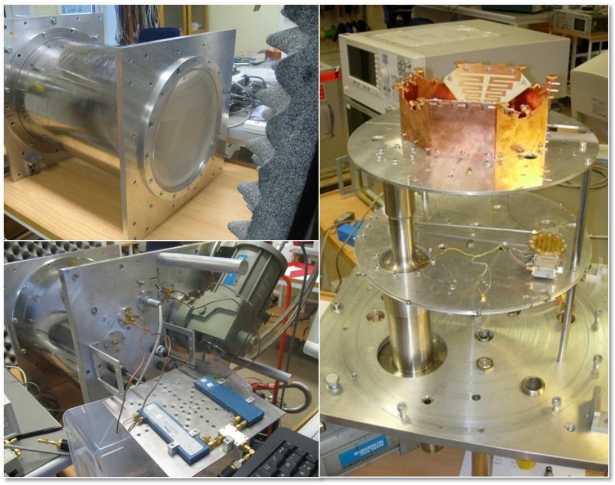

Fig. 9. Three photos of cryostat designed to house Eleven feed with integrated LNAs. Interior of cryostat in vertical position showing how Eleven feed is located (right). Complete cryostat in horizontal position (left) showing also the 0.35 mm thick Mylar window through which the Eleven feed "radiates" (upper left), and setup for measuring reflection coefficient of Eleven feed in cryostat (lower left).

IV. Descrambling and LNA-integration Alternatives

The dual-polarized Eleven feed has four log-periodic dipole array petals, each one with its own balanced 200 ohm port. In the previous low frequency models of the Eleven antenna [6][7], oppositely-located dipole petals were made of one metal piece, bent at two places to form two tilted petals joined together at the center, and thereafter mounted on the front side of the ground plane with a thin dielectric spacer to the center of the ground plane. The two orthogonal petals were made in the same way and mounted in a similar way on top of the central part of the metal piece of the first two petals with a dielectric spacer between them. However, this approach does not work well at high frequency [8], and the center puck was developed to solve this problem.

The center puck consists of four twin lead lines which guide the signal received by the antenna from the petals to the rear side of the ground plane. Each of the twin leads is coupled directly to the descrambler board (right pane of Fig. 1) where the ports are appropriately combined i.e. the descrambling and integration with the LNAs. The descrambling and LNA integration scheme therefore can be changed without disconnecting the dipole petals from the center puck.

Three descrambling and LNA integration schemes proposed here provide flexibility for different scenarios (test purpose, types of LNAs and other conditions), which are discussed in detail below.

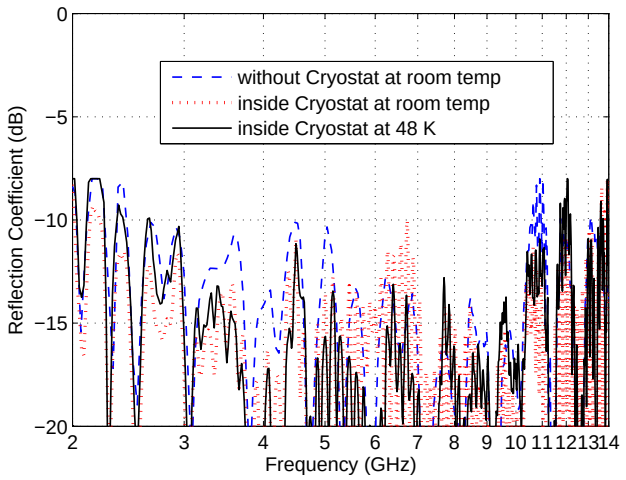

Fig. 10. Measured reflection coefficients of the cryogenic test model of the Eleven feed.

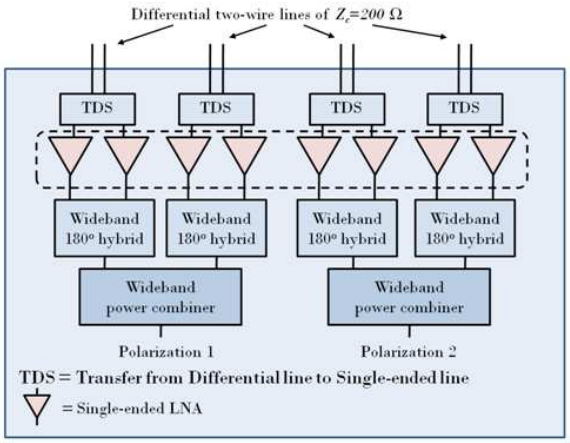

Fig. 11. Block diagram of descrambling using single-ended 8-port solution with commercial wideband 180° hybrid and 3 dB power combiner. This is mainly intended for testing purpose with eight coaxial ports, but can include single-ended LNAs connected to each port as illustrated. TDS is a transition from balanced twin-lead line to single-ended line.

A. Single-ended 8-port Solution with Center Puck

The single-ended 8-port solution with single-ended 50 ohm LNAs as a complete Eleven feed system is shown schematically in Fig. 11. It consists of a rear circuit board with eight coaxial ports and separate coaxial 180° hybrids and power combiners. Commercially available wideband 180° hybrids are lossy, and therefore should be preceded by the LNAs in order to avoid an unacceptable increase in the system noise temperature. This scheme is mainly intended for test purposes. For such tests, it is used without the LNAs in all the Eleven feed models described in Section III, and with 4 single-ended 50 ohm LNAs in the single-polarization noise measurements reported in Section VI. The dashed box around the LNAs in Fig. 11 indicates that they can be left out. Additionally, the eight ports can be combined in other ways for other purposes,

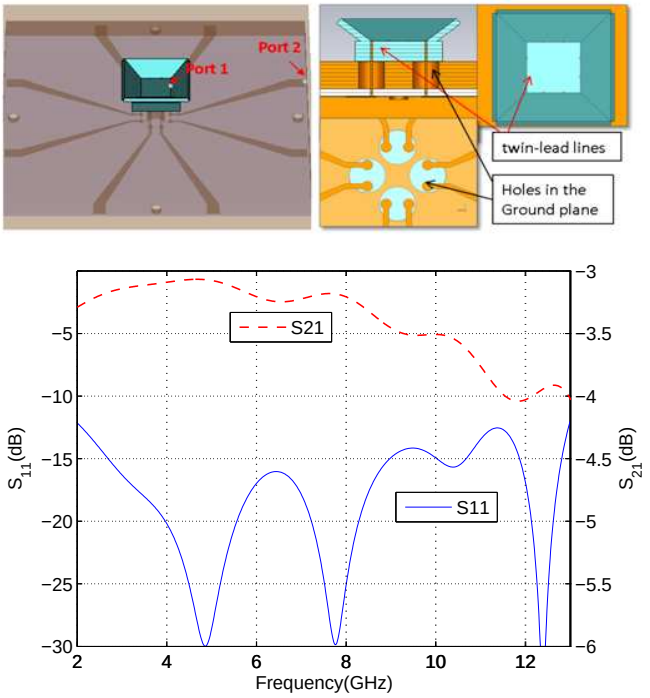

Fig. 12. Drawings of center puck and 8-port circuit board, and computed S-parameters. In the left drawing the geometry is shown with the ground plane removed. The right three drawings show different cuts and projections of the center puck: a vertical section of part of center puck (upper left), top view of center puck (upper right), and bottom view of connection to microstrip lines on the descrambling board.

such as tracking beams [9] in terminals and as monitoring antennas in satellite communication systems. This solution thus provides the most flexibility.

The center puck and 8-port circuit board are shown in Fig. 12, where there are four vertical twin-lead lines, each one made of two silver-plated steel needles. Each needle is soldered at one end to each of the metal strips feeding the log-periodic dipole arrays above the ground plane, and at the other end to a corresponding microstrip line on the descrambling board. The latter forms four pairs of coupled microstrip lines with 200 ohm odd mode impedance equal to the differential impedance of the two-strip lines feeding the dipoles on the front side of the ground plane. The dimensions of the parallel steel needle lines (separation, needle diameter and ground plane hole diameter) as well as the coupled line dimensions (separation and strip width) are matched such that parallel wires get soldered at the center of strips, and simultaneously give a 200 ohm characteristic impedance. The coupled microstrip lines are gradually separated by linear tapering, so as to get two separate uncoupled out-of-phase microstrip lines. The complete layout of the descrambling board and the simulated S-parameters are shown in Fig. 12. In the figure, port 1 is defined as the balanced port of one of the log-periodic dipole arrays, and port 2 is one of the corresponding 50 ohm microstrip ports on the 8-port circuit board. Since power is divided equally between the two 50 ports, S21 is ideally -3dB. There is a reduction due to the mismatch factor as shown by the dashed line in Fig. 12. The

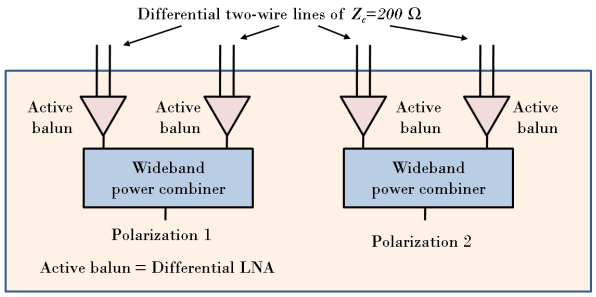

Fig. 13. Descrambling using four active baluns, i.e. differential LNAs with single-ended outputs.

Fig. 14. The active cryogenic balun developed at Caltech mounted in module. Differential input (200 ohms) at right and coaxial output (50 ohms) at left.

S21 in the figure is even lower than the mismatch factor, by an amount that increases with frequency. This indicates ohmic and radiation losses, and in this case turns out mainly to be radiation losses [28]. Thus, the present center puck suffers from radiation losses above 10 GHz. A solution to this problem was proposed in [28] by shielding the twin-lead lines, when they come through the ground plane on the front side, i.e. when they come through the center puck and connect to the dipole petals. This center puck radiation may also be the reason for the reduced BOR_1 efficiency observed above 10 GHz as explained in Section III. Other recent work on matching the rear circuit board was discussed in [31].

B. Active Balun Solution

The active balun descrambling solution is shown in Fig. 13. The cryogenic wideband differential LNA shown in Fig. 14 has been developed at Caltech based on an InP MMIC, and can be used as the active balun. There also exists a room temperature LNA on InP HEMT MMIC, developed at Chalmers, with a very similar mechanical lay-out that will be prepared for use and could be an option, even at cryogenic temperatures. The input port of the differential LNA is a coupled microstrip line with an odd mode characteristic impedance of 200 ohm, which is matched to the differential twin-lead lines used in the center puck. The output port of the differential LNA is a coaxial cable with a characteristic impedance of 50 ohm. After the four active baluns, two wideband power combiners (or hybrids, depending on the geometry of the LNAs) are used to form the outputs for dual linear polarizations.

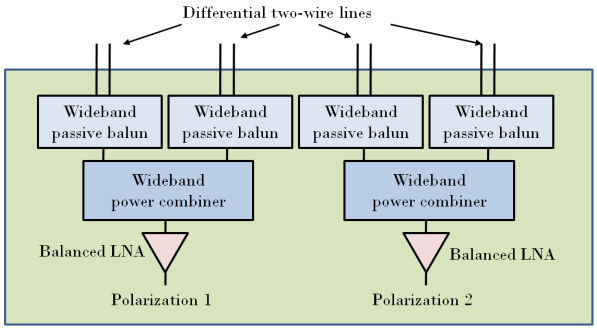

Fig. 15. Descrambling using four passive baluns and single-ended LNAs.

The major advantages of this descrambling solution are the following. First, the ohmic loss between the dipole petals and the LNAs is minimized, due to the direct integration of the Eleven antenna with the LNAs via the center puck. Second, the performance of the wideband power combiner (or hybrid) is not so critical as it is after the LNAs. Third, the solution is very compact in size.

There is ongoing work to develop low loss wideband power combiners at Chalmers [35]. We have seen reflection coefficients below -12 dB over the entire frequency range of 2 - 14 GHz, which is certainly acceptable.

The major challenges for this solution are the following two: the two differential LNAs of each polarization must be identical, and the common mode noise level must be suppressed. The first requirement assures good radiation performance of the feed, and reduces the common mode excitation. The second requirement assures that if the common mode of the feed is excited, the system noise temperature does not increase much.

C. Passive Balun Solution

Fig. 15 shows the block diagram of a passive balun descrambling solution. Four wideband baluns are connected directly to the four twin-lead lines. One wideband power combiner and a wideband cryogenic single-ended LNA are used to generate the single output port for each polarization.

Compact, low-loss and cryogenic coolable baluns with 2 - 14 GHz bandwidth, or similar, are not commercially available. Many ultra-wideband baluns have been reported in the literature, such as multiple-stage balun in [32], and microstrip-to-CPS transition in [33] and [34]. However, the multiple-stage balun in [32] is bulky, and the UWB baluns in [33]-[34] have insertion losses of around 1 dB at 13 GHz and high common mode level, which are unacceptable for this work. Other published baluns do not fit to our requirements of being integrated in a shielded package.

Therefore, we have a project at Chalmers to investigate the possibility of designing a compact, low-loss and cryogenic coolable balun. So far we have achieved a very compact balun with a simulated reflection coefficient below -10 dB from 3 to 13.5 GHz and the insertion loss of 0.5 dB, see [35] and [36]. This corresponds to a relative bandwidth of 4.5:1, and

work is ongoing to achieve the same 7:1 bandwidth as for the radiating dipoles, and to package them in a shielded enclosure.

This solution has several advantages. First, only two single-ended LNAs are needed per polarization, and not required to be identical. Second, the above-mentioned wideband passive balun has 20 dB common mode suppression, due to its symmetrical geometry [35]. Third, the LNAs can be disconnected from the descrambling board without changing the convenient 50 ohm port impedance. The antenna itself can, thereby be tested very easily without LNAs.

On the other hand, compared to the active balun descrambling, the ohmic losses and mismatch factor of the passive baluns and the power combiners will increase the noise temperature of the system. At cryogenic temperature, the mismatch loss is the larger of the two, therefore improvement of the reflection coefficients of the passive balun, and power divider over 2 - 14 GHz, is emphasized in further research.

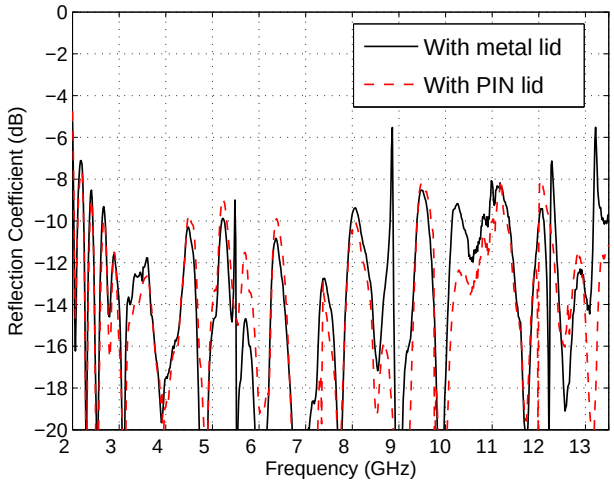

Fig. 16. Measured reflection coefficient of the Vertex model Eleven feed with the metal lid and the lid of nails for the 8-port circuit board solution.

D. Packaging Using Lid of Nails

The packaging is an important issue in the design of the descrambling circuits, with or without integrated LNAs. Due to the nearly decade bandwidth of the operating frequency, cavity modes are present in normal metal box packages, which destroy the performance. A new packaging technology, a lid-of-nail packaging, has been developed at Chalmers, and has been applied in a design of the 8-port circuit board used in the Eleven feed models described in Section III and shown in Fig. 1 and Fig. 12. The cavity modes can be suppressed by using this lid of nails, i.e. a metal box with a metal lid having metal pins or nails in it, as proposed in [37]. The suppression technique is based on the concept of gap waveguides [38], where stopbands are generated in the gap between parallel metal plates by providing one of the plates with a high surface impedance (the nail surface).

The lid of nails for the descrambling board is shown later in Fig. 18. Fig. 16 shows the measured reflection coefficients of the Vertex model of the Eleven feed according to (1), both when the descrambling board is packaged with a smooth metal lid and a lid of nails. We see clearly how cavity resonances at 5.5 GHz, 8.9 GHz, 12.3 GHz and 13.2 GHz are removed by the lid of nails.

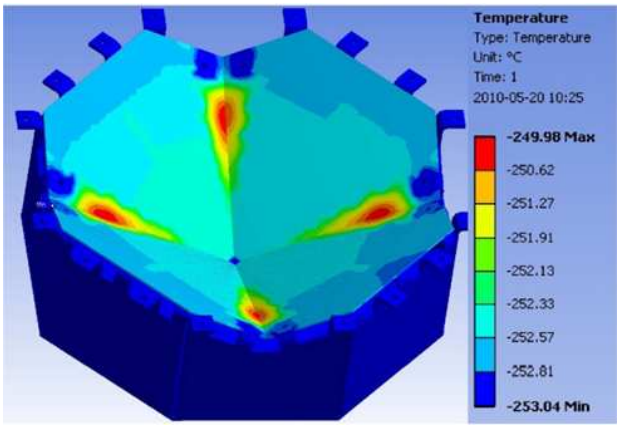

Fig. 17. Steady state analysis of the thermal distribution along the feed with head load of 20W/m2. The temperature difference between cold blue parts ($-253\ ^\circ C$) and hot red spots ($-249\ ^\circ C$) is about 4K.

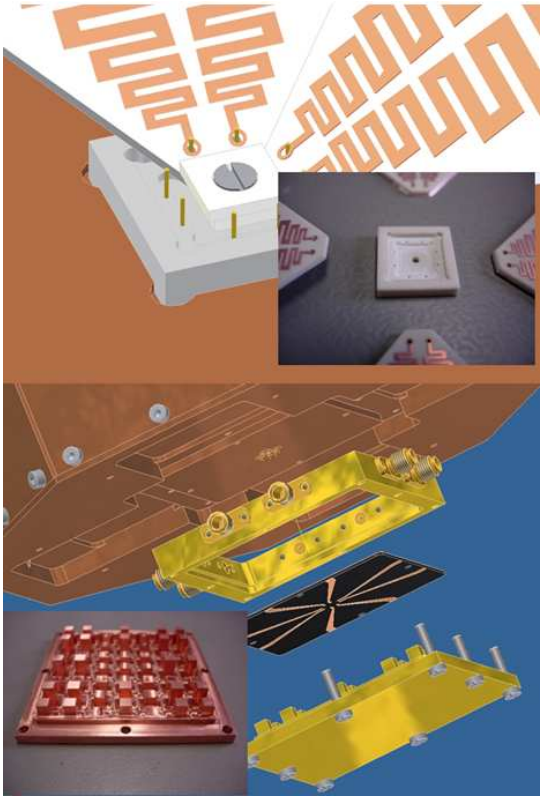

Fig. 18. CAD drawings of the center region with a specially shaped "center puck" milled from TMM3 serving as support for the petals and guide for the four twin needle lines, and of the rear side of the ground plane with the 8-port rear circuit board and the lid of nails.

V. Mechanical and Cryogenic Design and Testing

The cryostat integration of the previous 1-10 GHz Eleven feed, which was manufactured on a Pyralux AP film (Kevlar)

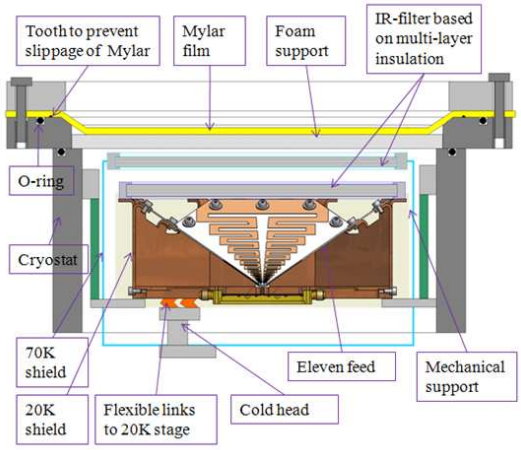

Fig. 19. Integration of the Eleven feed in cryostat for low noise receiver application.

and supported by Rohacell foam [8], showed a number of problems: deformation of the thin metal foil which forms folded dipoles, difficulty cooling the antenna due to the big volume of the foam support, unstable and problematic interface of the antenna to the center puck and the circuit board underneath the ground plane in terms of both the electrical and mechanical performance. The main objective of the mechanical and cryogenic design of the present Eleven feed was therefore to develop a mechanically stable construction that allows the petals of the Eleven antenna to be cooled down to cryogenic temperatures, without significant deformation of the geometry.

Therefore, we chose to use a microstrip laminated circuit board with good thermal performance. The main factors considered when selecting the dielectric substrate were low permittivity, thermal expansion coefficient (to match that of copper), and minimal deformation when cooled down to cryogenic temperatures. After a few preliminary tests, the TMM3 material from Rogers [39] was chosen. A compromise between the thickness of the dielectric material and the copper is also required. Extensive cryogenic simulations of different geometries show that a dielectric thickness of 0.76mm and copper cladding of 70um are suitable to provide cooling of the feed and still maintain excellent mechanical stiffness.

Fig. 17 shows the simulated temperature distribution along the surface of the petal generated through a steady-state thermal analysis by using the 3D solver - ANSYS [30]. In this analysis, the last dipole and the area next to the twin lead line are terminated at 20K.

Fig. 18 shows the final CAD drawings of the center puck region and the integration of the descrambling board with the lid of nails.

The cryostat developed to conduct measurements of the system noise temperature has already been shown in Fig. 9. Fig. 19 shows a cross section of its interior, and how the Eleven antenna is integrated.

VI. Figure of Merit and System Noise Temperature

Commonly, the achievable SNR (signal to noise ratio) performance of a radio telescope can be expressed by a single figure of merit A/T. In the present estimation, we normalize A/T to an antenna area of one square meter physical reflector aperture, in order to get a comparative performance measure independent of antenna size. This can then be expressed as

$$(A/T)_{/m^2} = \frac{A/T}{A_{ph}} = \frac{A_{ph} \cdot e_{ant}/(T \cdot A_{ph})}{A_{ph}} = \frac{e_{ant}}{T_{SYS}} \quad (2)$$
$$e_{ant} = e_{ap} e_{rad}$$

where A_{ph} is the aperture area of the antenna, e_{ant} the antenna efficiency, T_{SYS} the total system noise temperature, e_{ap} the aperture efficiency of the reflector, and e_{rad} the radiation efficiency of the feed due to ohmic losses, excluding the mismatch factor. The mismatch factor is omitted, because it is of the convention to include it in the T_{SYS} quantity instead, being consistent with the noise model block diagram in Fig. 20(a) [40]. In this way, the A/T ratio will be the same, independent of where it is evaluated in the receiver chain. The model assumes that the LNA input impedance is 50 ohms.

The applied system noise model uses the equivalent system representation in Fig. 20a (for one polarization), obtained from [40], according to which the 4-port Eleven feed is replaced by an equivalent single port antenna and the multi-channel receiver including 2 differential LNAs (or 4 single-ended LNAs and two 180 deg hybrids) is replaced by one equivalent LNA. The 4 loads and the power combiner represent a 'passive beamforming network'. This simplification is allowed provided the LNAs (and 180 deg hybrids) are identical and have high enough gain to remove the noise contributions from the power combiner (and 180 deg hybrids). It is also assumed that no noise is coupled from the loads on the ports of the orthogonal polarization. The measured results to be presented in Section VI-C indicate that the assumptions are valid.

The reference plane for the system noise temperature model is shown in Fig. 20(a). The reference plane is considered to be located at the input port of the LNA, however, the impedance mismatch between the feed and LNA is included as a separate box between the LNA and the reference plane. The reason for this separation is that this mismatch causes a change in both the noise temperature and power gain of the LNA, and thus belongs as a block between the LNA and the reference plane, according to the convention described above.

The overall system noise temperature, T_{SYS}, can now be expressed according to Fig. 20(a) as:

$$T_{SYS} = T_{ext} e_{rad} + T_{ohmic} + L_{LNA}$$
$$T_{ohmic} = (1 - e_{rad}) T_{PhFeed} \quad (3)$$

where T_{ext} is the noise contribution due to external noise sources (ground and sky), T_{PhFeed} the physical temperature of the feed, T_{ohmic} the noise contribution due to the ohmic losses in the system in front of the LNAs, and T_{LNA} the LNA noise temperature. The power gain of the LNA is assumed to be so large that the noise due to the physical temperature of the power combiners behind the LNA can be ignored. The

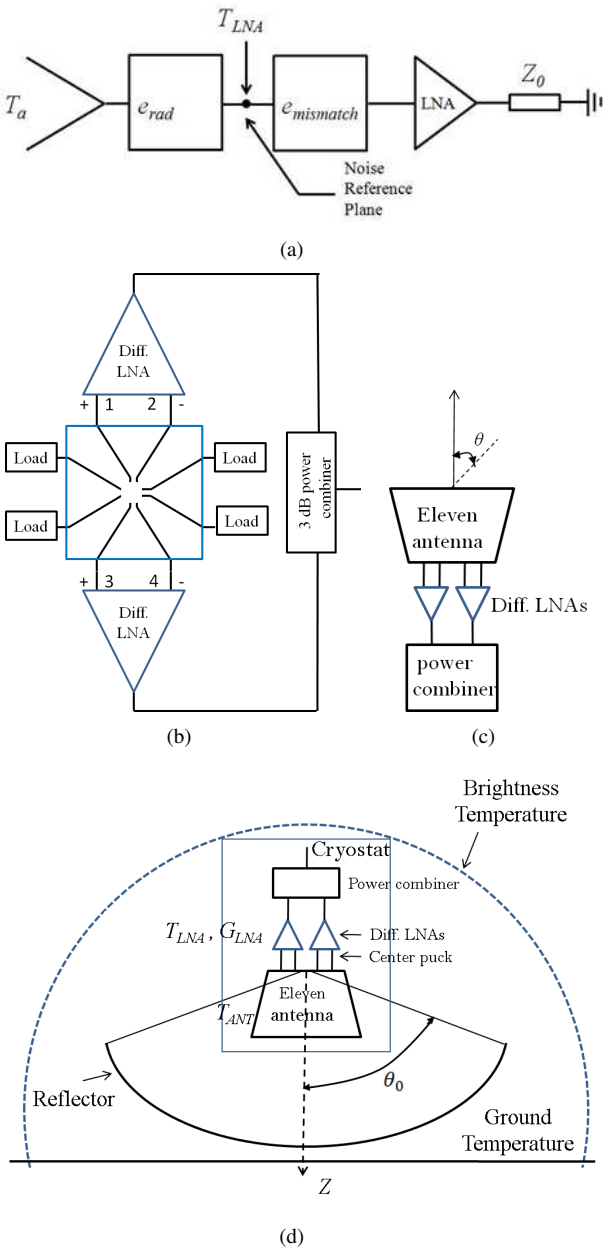

Fig. 20. Illustrations of noise models and test scenarios. a) Block diagram representing the A/T and noise models with reference plane. b) Configuration of LNAs and power combiner network for single polarization noise temperature tests. c) Sketch showing feed pointing upwards for evaluating antenna noise temperature under test conditions. d) Sketch showing feed pointing downwards towards reflector for evaluating noise temperature during operation in radio telescope.

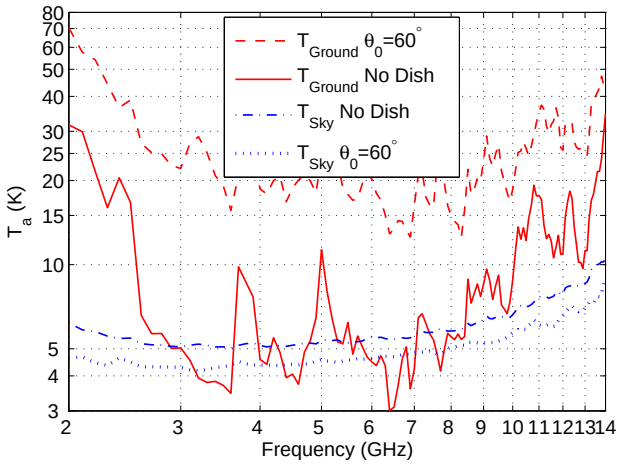

Fig. 21. Antenna noise temperature contributions from the sky and ground for the two scenarios in Figure 20c and d. The calculations are based on complete measured radiation patterns of the Vertex model (not located in cryostat). TPhFeed = 30 K.

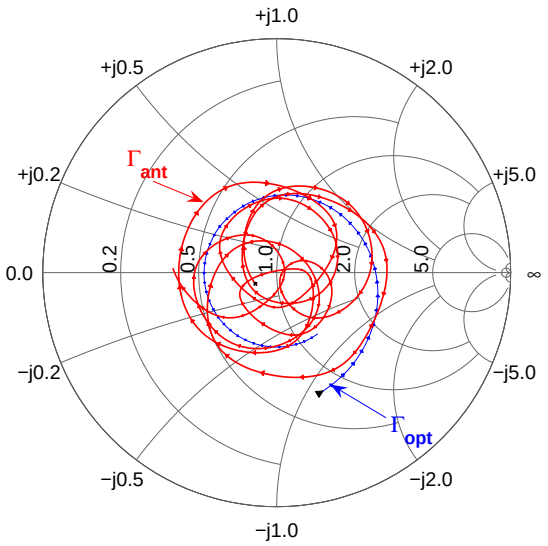

Fig. 22. Γ_{ant} and Γ_{opt} relative to 50 ohm, both plotted over the reduced range 4-8 GHz for clarity.

LNAs used for the noise temperature tests possess a gain of more than 30 dB between 2 and 12 GHz, see Section VI-B.

In the rest of this section, we will explain how the noise temperature of the cryogenic Eleven feed system can be estimated with an 8-port circuit board and single-ended LNAs.

A. Antenna Noise Temperature

Fig. 20(c) and Fig. 20(d) show the two geometrical scenarios used for the noise temperature analysis; one in which the feed looks at zenith, and the another in which the feed is located inside a reflector which points towards zenith. The first scenario is valid for the noise tests described in Section VI-C. The second scenario represents the configuration of the radio telescope used to predict the A/T in Section VI-D. The second scenario represents a worst case noise temperature performance because spillover from the feed is intercepted by the 290 K ground plane when the main beam of the telescope points towards zenith.

The external noise temperature contribution T_{ext} seen by

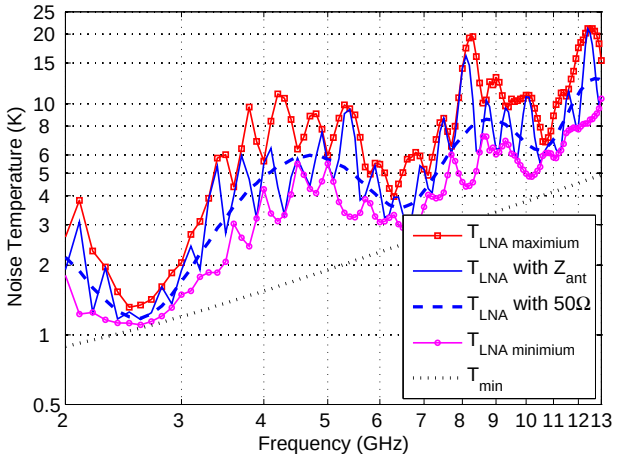

Fig. 23. Noise temperatures of the 4 single-ended Caltech HEMT LNAs used for the noise temperature tests, when connected to the Eleven antenna.

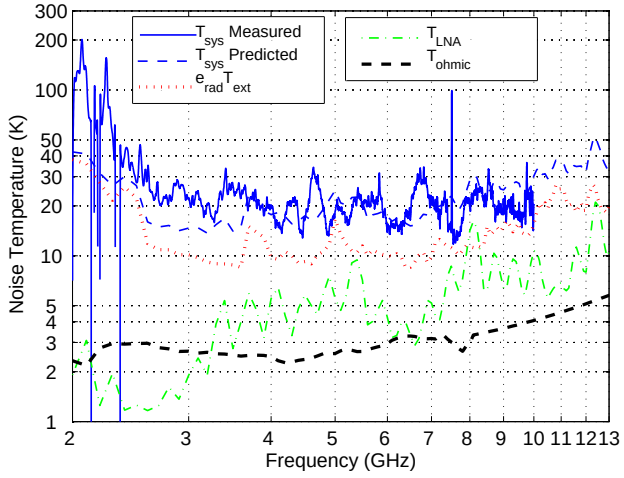

Fig. 24. Measured and predicted system noise temperatures when the cryostat with Eleven feed is pointing vertically directly towards the sky. The measurements were done at Haystack Observatory. The different contributions to T_{sys} in (3) are also shown.

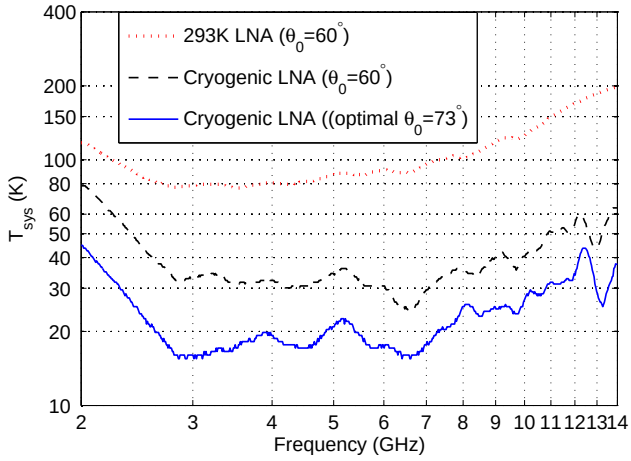

(a)

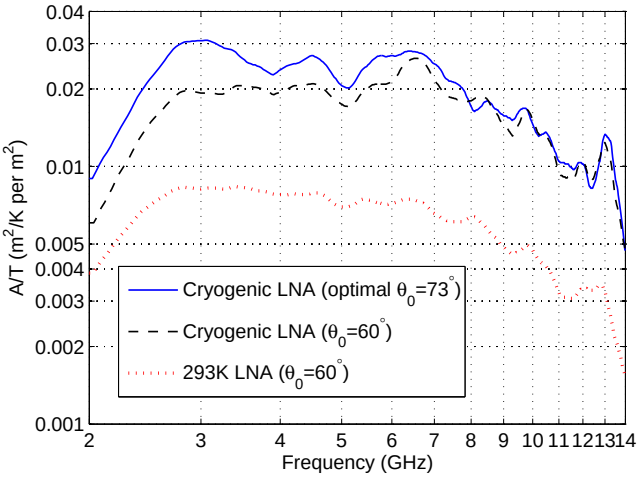

(b)

Fig. 25. Estimated system noise temperatures (upper graph) and A/T per m2 (lower graph) of Eleven feed with 4 single-ended LNAs, when located in cryostat and cooled to 30 K, and feeding a paraboloid with semi-subtended angles of 60° and 73°, respectively.

the antenna is defined by [41]

$$T_{ext} = \frac{\iint_{4\pi} T_{bg}(\theta_f)[|G_{CO}(\theta_f,\varphi_f)|^2 + |G_{XP}(\theta_f,\varphi_f)|^2]\sin\theta_f d\theta_f d\varphi_f}{\iint_{4\pi} [|G_{CO}(\theta_f,\varphi_f)|^2 + |G_{XP}(\theta_f,\varphi_f)|^2]\sin\theta_f d\theta_f d\varphi_f} \quad (4)$$

where the integration is chosen over the copolar $G_{CO}(\theta_f,\varphi_f)$ and crosspolar $G_{XP}(\theta_f,\varphi_f)$ radiation field functions of the feed, and T_{bg} a combination of the ground temperature T_g and the sky brightness temperature T_b. We separate T_{ext} in two contributions in order to study the relative importance of the sky (i.e. T_b) and ground noise (T_g), according to

$$T_{ext} = T_{Sky} + T_{Ground}. \quad (5)$$

These are then computed by separating the integral in (4) into the T_b and T_g contributions as

$$T_{bg}(\theta_f) = \begin{cases} T_b(\theta_f), & 0 \le \theta_f \le \pi/2 \\ T_g(\theta_f), & \pi/2 \le \theta_f \le \pi \end{cases} \quad (6)$$

for the scenario in Fig. 20(c) and

$$T_{bg}(\theta_f) = \begin{cases} T_b(zenith), & 0 \le \theta_f \le \theta_0 \\ T_g(\theta_f), & \theta_0 \le \theta_f \le \pi/2 \\ T_b(\theta_f), & \pi/2 \le \theta_f \le \pi \end{cases} \quad (7)$$

for the scenario in Fig. 20(d), where $T_b(zenith)$ is T_b in the vertical direction (at zenith). The angle θ_0 is the subtended half angle of the reflector, as seen in Fig. 20(d).

In the operating frequency range of the Eleven feed, it is possible to use the atmospheric noise models published in [42] and [43], which fully describes the atmospheric brightness as a function of frequency and elevation angle. The ground contribution can be considered constant and equal to 290 K by convention, thereby assuming that the ground is an absorbing object with reflection coefficient zero. Using these

models, we have computed the antenna noise temperatures T_{Sky} and T_{Ground} for the two scenarios shown in Fig. 20(c) and Fig. 20(d), and plot the results in Fig. 21. We see that the ground noise is large below 2.7 GHz and above 10 GHz. Further studies show that the poor low frequency performance is due to the widening of the beam and low BOR_1 efficiency below 2.7 GHz. This is caused by the vertical support walls of the dipole petals and the finite size of the ground plane. Increased back radiation and spillover causes also the increased noise level above 10 GHz. The values of the BOR_1 efficiency and spillover are good indicator of the degradation of the antenna noise temperature, being low both below 2.7 GHz and above 10 GHz.

The noise contribution due to ohmic losses amounts to 7 K per 0.1 dB in room temperature, but it is a factor of 10 smaller when the feed is cooled down to 30 K. Therefore, the noise contribution due to the radiation efficiency e_{rad} (shown in Fig. 24) will be a maximum of 3 K.

B. LNA Noise Temperature

The LNA noise temperature can be calculated from the common expression [44]:

$$T_{LNA} = T_{min} + 4NT_0 \frac{|\Gamma_{ant} - \Gamma_{opt}|^2}{(1-|\Gamma_{ant}|^2)(1-|\Gamma_{opt}|^2)} \tag{8}$$

where Γ_{ant} is the antenna reflection coefficient seen at the reference point (due to the impedance mismatch), and T_{min}, N, and Γ_{opt} are the LNA noise parameters as defined e.g. in [44]. T_0 is the standard temperature of 290 K. From (7), it is clear that the minimum noise temperature is achieved when $\Gamma_{ant} = \Gamma_{opt}$, where Γ_{opt} is the optimal antenna (i.e. source) reflection coefficient at which the LNA noise temperature has its minimum T_{min}. The factor N determines how sensitive the noise temperature is to deviations from this optimum noise match.

The present tests were done with 4 single-ended 50 ohm cryogenic InP HEMT LNAs developed at California Institute of Technology (Caltech), based on the design in [45] with specifications given in [46]. The frequency band is 2-12 GHz over which the gain is 32 ± 2 dB, and the average noise temperature, when cooled to 11 K, is 6 K. The noise sensitivity constant N varies between 0.001 and 0.01 from 1 to 20 GHz, and T_{min} between 1 K and 4 K (see Fig. 23). The minimum noise reflection coefficient Γ_{opt} is plotted together with the antenna reflection coefficient Γ_{ant} in Fig. 22 over a reduced frequency range (4-8 GHz) for clarity, both being normalized to a characteristic impedance of 50 ohm. From the figure, it can be concluded that the impedance noise match ($\Gamma_{ant} = \Gamma_{opt}$) between the Eleven antenna and LNA cannot be achieved except at specific frequency points, because the impedance of the Eleven feed varies with frequency at a much higher rate compared to that of the LNA, and, the Eleven feed acts inductively, while the LNA acts capacitively, so that they rotate in opposite directions in the smith chart, as shown in Fig. 22.

The rotations of Γ_{opt} and Γ_{ant} over the frequency band in opposite directions in the Smith chart cause T_{LNA} to vary periodically between minimum value given from (7) using $|\Gamma_{ant} - \Gamma_{opt}| \geq ||\Gamma_{ant}| - |\Gamma_{opt}||$ and maximum using $|\Gamma_{ant} - \Gamma_{opt}| \leq |\Gamma_{ant}| + |\Gamma_{opt}|$. It is not possible to predict the detailed variations in T_{LNA}, due to the uncertainty associated with predicting and measuring Γ_{opt}, Γ_{ant} and N. For example, the Γ_{ant} and the radiation efficiency e_{rad} were measured in free space instead of in the cryostat, so that the window and walls of the cryostat are not accounted for. However, the predicted maximum and minimum values, according to

$$\begin{aligned} T_{LNAmin} &= T_{min} + 4NT_0 \frac{(|\Gamma_{ant}| - |\Gamma_{opt}|)^2}{(1-|\Gamma_{ant}|^2)(1-|\Gamma_{opt}|^2)} \\ T_{LNAmax} &= T_{min} + 4NT_0 \frac{(|\Gamma_{ant}| + |\Gamma_{opt}|)^2}{(1-|\Gamma_{ant}|^2)(1-|\Gamma_{opt}|^2)}, \end{aligned} \tag{9}$$

will give envelopes within which the actual noise temperature variation is much less sensitive to uncertainties. Therefore, the maximum and minimum T_{LNA} values are plotted in Fig. 23 for the above-mentioned single-ended Caltech LNAs. Also shown in Fig. 23 are the predicted T_{LNA} values for the cases when the LNA input port is terminated with measured antenna impedance Z_{ant} and with an ideal 50 ohm load. The latter case corresponds to matching the Eleven antenna input impedance perfectly to 50 ohms. Based on the results shown in Fig. 23, we see that over most of the band below 8 GHz there is no significant enhancement in the noise performance by improving the Eleven antenna's input impedance match to 50 ohms. A major contributor to the uncertainty is that the measured LNA noise parameters do not include the effect of the coaxial connector.

C. Measured and Estimated T_{sys} for Feed Pointing towards Zenith

System Y-factor noise measurements were performed at MIT Haystack observatory by using 4 single-ended 50 ohm InP HEMT LNAs from Caltech, connected to the 4 feed ports of one polarization of the Statkart model as shown in Fig. 20(b). The 4 ports of the other polarization were terminated with 50 ohm loads. This means that each of the 2 differential LNAs in Fig. 20 b, c and d were replaced by two single-ended LNAs and a 180 deg hybrid. The noise model is still valid under the conditions and assumptions explained in the second paragraph of Section VI. The outputs of the 4 LNAs were connected to 180° hybrids and power combiners as shown in Fig. 20(b). The results of the measurements and predictions using the above model in (7) are shown in Fig. 24. The system noise temperature averaged over 2.7 to 10 GHz is 20.7 K in the measured case, and 20.5 K estimated by the above formulas, which is a quite remarkable agreement. The reason for the increased noise temperature above 10 GHz was studied and found to be the reduced BOR_1 efficiency that causes significant back radiation. The increase below 2.7 GHz is due to the widening of the beam and reduced BOR_1 efficiency at low frequencies. There are some narrow dips and peaks in the measured noise temperature curves, in particular below 2.7 GHz, but these are typical for interference from external transmitters (RFI). Note also that the noise temperature estimates were done based on feed patterns measured without cryostat, whereas the measured

noise temperatures were done with cryostat. This causes a significant uncertainty at low frequencies.

D. Estimated Figure of Merit A/T of Feed in Reflector

Fig. 25 presents the estimated performance when the Eleven feed is located in a parabolic reflector pointing upwards towards zenith, i.e. the scenario in Fig. 20(d) described by (7). The same 8-port circuit board and LNAs analyzed in Section VI-C were used in this noise analysis. As shown in Fig. 25, the A/T ratio is optimized for a subtended angle of about $\theta_0 = 73°$, and we also present results for $\theta_0 = 60°$ for showing that the difference is small. For reference, the SKA has a goal of a system noise temperature of 35 K over an antenna area of a square kilometer, corresponding to $(A/T)_{/m^2} = 0.02$ m^2/K per m^2 which we match well between 3 and 7 GHz. For comparison we have also shown the performance of the uncooled case, using the same LNAs at 293 K.

VII. Conclusions and Ongoing Further Developments

The paper describes an Eleven feed system that works well for use in future wideband radio telescopes, having constant beamwidth, constant phase center location and high aperture efficiency between 2 and 13 GHz (> -3 dB). The goal was to reach 14 GHz, but there are strong degradations above 13 GHz. The degradations can be seen to start gradually from 10 GHz by observing the BOR_1 efficiency, and this subefficiency drops abruptly above 13 GHz. Ongoing research indicates that this degradation is caused by radiation from the center puck that excites surface waves in the dielectric support for the log-periodic dipole petals. The BOR_1 efficiency as defined in [26] has proven to be a valuable diagnosis tool for non-axially symmetric feeds for reflectors, in the same way as it was during the developments reported in [10].

There is also a minor deficiency in the feed performance below 2.5 GHz, which is believed to be associated with the mechanical support structure of the dipole petals. This can be solved in the next generation of feeds by a more thorough modeling of the support structure. We also believe that it is possible to reduce the size of the Eleven feed, because the outer 2 dipole pairs are only included to appropriately terminate the log-periodic structure. They do not significantly contribute to the radiation. Therefore, it might be possible to redesign the outer part in a more compact way.

The project has involved mechanical and cryogenic design of the feed and the cryogenic housing. This has been successful, in the sense that the feed has been demonstrated to work when cooled to 48 K, and it can survive even colder temperatures. This testing has been done by means of a cryostat designed to be used together with the feed. This will be used for further testing with integrated LNAs.

The feed system is provided with a flexible descrambling solution on the rear side of the ground plane with a circuit board that can be interchanged to facilitate different LNA integration schemes. Three such schemes have been described in this work.

The system noise temperature and A/T were predicted based on the computed and measured results of the presented Eleven feed models. The increased noise temperature due to noise impedance mismatch between the LNA and Eleven feed was accounted for as was the pick-up of ground noise. Measurements have been performed at Haystack Observatory by pointing the cryostat with feed vertically towards zenith, and we were able to compute the same system noise temperature as measured between 2.7 and 10 GHz. The ripples in the curves do not appear at the same frequencies, but the average noise temperature differs only by 0.2 K over this frequency band, which makes us believe that the system noise model is quite accurate. To get control of the ripples we need an even better noise model. The increased system noise temperature below 2.7 GHz and above 10 GHz can be explained by reference to the BOR_1 efficiency and the spillover.

The predicted A/T ratio coincides with the 0.02 m^2/K per m^2 goal of SKA over the frequency range 2.7 - 8 GHz. The tests were performed with single-ended 50 ohm LNAs purchased from Caltech, but we believe that even better results can be achieved with differential LNAs. Integration and tests with differential LNAs are being planned in the near future.

The Eleven feed is protected by a pending patent [47].

Acknowledgment

This work has been supported in part by The Swedish Foundation for Strategic Research (SSF) within the Strategic Research Center CHARMANT. The hardware development in this work was funded partly by The Swedish Governmental Agency for Innovation Systems (VINNOVA) within a so-called VINN Verification project, and via hardware orders from Vertex Antennentechnik GmbH in Germany and the Norwegian Mapping Authority Statkart. Onsala Space Observatory has contributed in-kind with the cryogenic design, fabrication of the test cryostat, and cryogenic tests. The system noise temperature studies were supported by the Swedish research links program of Swedish Research Council VR and SIDA, and by NRF in South Africa. The measurements of radiation patterns were performed at Technical University of Denmark (DTU) by Sergei Pivnenko. There were also contributions to the evaluation of the electrical performance from Sander Weinreb at California Institute of Technology (Caltech), who provided the single-ended LNAs used for the noise temperature tests. Finally, we are thankful to Marianna Ivashina and Rob Maaskant from Astron for discussions regarding modeling of the system noise temperature.

References

[1] P. Hall, *The SKA: An Engineering Perspective*, Springer, 2005.
[2] A. Niell, A. Whitney, W. Petrachenko, W. Schlter, N.Vandenberg, H. Hase, Y. Koyama, C. Ma, H. Schuh, G. Tuccari, "(2005) VLBI2010: Current and Future Requirements for Geodetic VLBI Systems," *IVS WG3 Report*, http://ivscc.gsfc.nasa.gov/about/wg/wg3.
[3] Z. N. Chen, "UWB antennas: from hype, promise to reality," *2007 Loughborough Antennas and Propagation Conference*, Loughborough, UK, 2 -3 April 2007.
[4] A. van Ardenne, *private communications*, at Chalmers, Dec 2009.
[5] R. Olsson, P.-S. Kildal and S. Weinreb, "The Eleven antenna: a compact low-profile decade bandwidth dual polarized feed for reflector antennas," *IEEE Trans. Antennas Propogat.*, vol. 54, no.2, pp. 368-375, Feb. 2006.

[6] R. Olsson, P.-S. Kildal, and M. Shields, "Measurements of a 150 to 1700 MHz low loss Eleven feed for the 42 m radio telescope at Green Bank," *IEEE AP-S International Symposium*, Albuquerque, N.M., July 2006.

[7] Y. B. Karandikar and P.-S. Kildal, "Optimization of 200-800 MHz Eleven feed for use in reflector antennas of GMRT," *The Second European Conference on Antennas and Propagation (EuCAP 2007)*, Edinburgh, 11 - 16 November 2007.

[8] J. Yang, X. Chen, N. Wadefalk, P.-S. Kildal, "Design and realization of a linearly polarized Eleven feed for 1-10 GHz," *IEEE Antennas Wireless Propag. Lett.*, vol. 8, pp. 64-68, 2009..

[9] J. Yin, J. A. Aas, J. Yang and P.-S. Kildal, "Monopulse tracking performance of multi-port Eleven antenna for use in terminals for satellite communications," *The Second European Conference on Antennas and Propagation (EuCAP 2007)*, Edinburgh, 11 - 16 November 2007.

[10] A. Yasin, J. Yang, T. Ostling, "A novel compact dual band feed for reflector antennas based on choke horn and circular Eleven antenna," *IEEE Trans. Antennas Propoga.*, vol. 57, no. 10, pp. 3300-3302, Oct. 2009.

[11] V. Rodriguez, "An open-boundary quad-ridged guide horn antenna for use as a source in antenna pattern measurement anechoic chamber," *IEEE Antennas Propoga. Mag.*, vol. 48, No. 2, pp. 157-160, Apr. 2006.

[12] G. Cortes-Medellin, "Novel non planar ultra wide band quasi self-complementary antenna," *Proc. of IEEE AP-S Symposium*, pp. 5733 - 5736, Honolulu, Hawaii, 9-15 June 2007.

[13] J. Yang, S. Pivnenko and P.-S. Kildal, "Comparison of two decade-bandwidth feeds for reflector antennas: Eleven antenna and quadridge horn," *The Fourth European Conference on Antennas and Propagation (EuCAP 2010)*, Barcelona, 12-16 April 2010.

[14] S. Bruni, A. Neto and F. Marliani, "The Ultrawideband leaky lens antenna," *IEEE Trans. Antennas Propag.*, vol. 55, no.10, pp. 2642-2653, Oct. 2007.

[15] J. Yang, S. Pivnenko, T. Laitinen and J. Carlsson, "Measurements of diversity gain and radiation efficiency of the Eleven antenna by using different measurement techniques in Etech project," *The Fourth European Conference on Antennas and Propagation (EuCAP 2010)*, Barcelona, 12-16 April 2010.

[16] Y. B. Karandikar, "Pattern studies of two parallel dipoles in eleven configuration above ground plane as feed for reflector antenna," *IEEE Antennas Wireless Propag. Lett.*, vol. 9, pp. 558-561, 2010.

[17] J. Yang, D. Nyberg, J. Yin, "Impedance matrix of a folded dipole pair under Eleven configuration," *IET Microw. Antennas Propag.*, vol.4, no. 6, pp.697-703, June 2010.

[18] J. Yang and P.-S. Kildal, "Optimization of reflection coefficient of large log-periodic array by computing only a small part of it," *IEEE Trans. Antennas Propag.*, vol. 59, no. 6, pp.1790-1797, June 2011.

[19] CST Microwave Studio, 3D EM Simulation software, www.cst.com.

[20] http://www.statkart.no/.

[21] http://www.vertexant.com/.

[22] http://www.astro.caltech.edu/.

[23] http://www.oso.chalmers.se/.

[24] J. Yang, "On conditions for constant radiation characteristics for log-periodic array antennas," *IEEE Trans. Antennas Propag.*, vol. 58, no. 5, pp.1521-1526, May 2010.

[25] P.-S. Kildal, "Factorization of the feed efficiency of paraboloids and Cassegrain antennas," *IEEE Trans. Antennas Propag.*, vol. 33, no. 8, pp.903-908, Aug. 1985.

[26] P.-S. Kildal, Z. Sipus, "Classification of Rotationally Symmetric Antennas as Types BOR0 and BOR1," *IEEE Antennas Propoga. Mag.*, vol. 37, no 6, p. 114, Dec. 1995.

[27] W. V. T. Rusch and P. D. Potter, *Analysis of Reflector Antennas*, New York: Academic, 1970.

[28] Y. B. Karandikar, J. Yang, P.-S. Kildal, "Reduction of radiation from central exciting region of Eleven feed and pattern improvements for VLBI 2010 applications," *The Fourth European Conference on Antennas and Propagation (EuCAP 2010)*, Barcelona, 12-16 April 2010.

[29] K. Rosengren and P.-S. Kildal, "Radiation efficiency, correlation, diversity gain, and capacity of a six monopole antenna array for a MIMO system: Theory, simulation and measurement in reverberation chamber," *Proceedings IEE, Microw. Antennas Propag.*, vol. 152, no. 1, pp.7-16, February 2005.

[30] http://www.ansys.com.

[31] Y. B. Karandikar, P.-S. Kildal, "Comparisons of different descrambler/ power combining boards layout for multi-port, decade bandwidth Eleven feed," *The Fourth European Conference on Antennas and Propagation (EuCAP 2010)*, Barcelona, 12-16 April 2010.

[32] S.-H. Ye and C.-Y. Chen, "A symmetric log-periodic balun for ultra-wideband application," *2007 IEEE Conference on Electron Devices and Solid-State Circuits (EDSSC 2007)*, Taiwan, December 20-22, 2007.

[33] Young-Ho Suh and Kai Chang, "A wideband coplanar stripline to microstrip transition," *IEEE Microw. Wireless Compon. Lett.*, vol. 11, no. 1, pp.28-29, Jan. 2001.

[34] Y.-G. Kim, D.-S. Woo, K. W. Kim, Y.-K. Cho, "A new Ultra-wideband Microstrip-to-CPS transition," *2007 IEEE MTT-S International Microwave Symposium*, Honolulu, Hawaii, 3-8 June 2007.

[35] A. Zamanifekri, "Design of power dividers and 180 deg hybrids for use with the Eleven antenna for VLBI2010 and SKA applications," *Master's thesis*, Chalmers University of Technology, May 2010.

[36] A. Zamanifekri and J. Yang, "Two octaves bandwidth passive balun for the Eleven feed for reflector antennas," *2010 IEEE international Symp. on Antennas Propag.*, Toronto, July 11-17, 2010.

[37] E. Rajo-Iglesias, A. Uz Zaman, P.-S. Kildal, "Parallel plate cavity mode suppression in microstrip circuit packages using a lid of nails," *IEEE Microw. Wireless Compon. Lett.*, vol. 20, no. 1, pp.31-33, Jan. 2010.

[38] P.-S. Kildal, E. Alfonso, A. Valero-Nogueira, E. Rajo-Iglesias, "Local metamaterial-based waveguides in gaps between parallel metal plates," *IEEE Antennas Wireless Propag. Lett.*, vol. 8, pp. 84-87, 2009.

[39] http://www.rogerscorp.com/.

[40] M. V. Ivashina, R. Maaskant, B. Woestenburg, "Equivalent system representation to model the beam sensitivity of receiving antenna arrays," *IEEE Antennas Wireless Propag. Lett.*, vol. 7, pp. 733-737, 2008.

[41] P.-S. Kildal, *Foundations of Antennas: A unified Approach*, Studentlitteratur, Lund, 2000.

[42] M. A. Jensen, "An introduction to the passive microwave remote sensing of atmospheres," *Atmospheric Remote Sensing by Microwave Radiometry*, John Wiley&Sons, New York, Ch. 1, 1993.

[43] X. Chen, "Study of system noise temperature from 50 MHz to 15 GHz with application to eleven antennas," *Master's thesis, ISSN 99-2747920-4*, Chalmers University of Technology, URL to fulltext: http://publications.lib.chalmers.se/records/fulltext/67232.pdf.

[44] M. W. Pospieszalski, "Modeling of Noise Parameters of MESFETs and MODFETs and their frequency and temperature dependence," *IEEE Trans. Microw. Theory Tech.*, vol. 37, no. 9, pp. 1340 - 1350, Sept. 1989.

[45] J. D. Pandian, L. Baker, G. Cortes, P. F. Goldsmith, A. Deshpande, R. Ganesan, J. Hagen, L. Locke, N. Wadefalk, S. Weinreb, "Low noise 6-8 GHz receiver," *IEEE Microw. Mag.*, pp. 74-84, Dec. 2006.

[46] "Technical data sheet, CITCRYO1-12,", available from sweinreb@caltech.edu.

[47] P.-S. Kildal, "Broadband multi-dipole antenna with frequency-independent radiation characteristics,", PCT patent application number PCT/SE2004/001178.

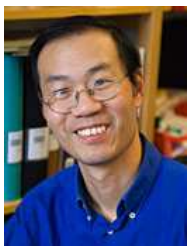

Jian Yang (M'02-SM'10) received the B.S. degree from the Nanjing University of Science and Technology, Nanjing, China, in 1982, and the M.S. degree from the Nanjing Research Center of Electronic Engineering, Nanjing, China, in 1985, both in electrical engineering, and the Swedish Licentiate and Ph.D. degrees from the Chalmers University of Technology, Gotherberg, Sweden, in 1998 and 2001, respectively.

From 1985 to 1996, he was with the Nanjing Research Institute of Electronics Technology, Nanjing, China, as a Senior Engineer. From 1999 to 2005, he was with the Department of Electromagnetics, Chalmers University of Technology as a Research Engineer. During 2005 and 2006, he was with COMHAT AB as a Senior Engineer. From 2006, he has been an Assistant Professor at the Department of Signals and Systems, Chalmers University of Technology. From 2010, he has been titled as Associate Professor. His research interests include ultra-wideband antennas, UWB radar systems, hat-fed antennas, reflector antennas, radome design, and computational electromagnetics.

Miroslav Pantaleev received the M.S. degree in electrical engineering from the Technical University of Sofia, Sofia, Bulgaria, in 1995, and the M.S. and Ph.D. degrees from the Chalmers University of Technology, Gteborg, Sweden, in 2000 and 2006, respectively.

During his doctoral studies, he was involved in beam measurement characterization for HIFI Instrument of Herschel satellite and later in the design and tests of the HEB mixer for the APEX telescope. He is currently the Head of the Operation and Development Laboratory, Onsala Space Observatory, Onsala, Sweden, where he is responsible for the design, integration, implementation, and testing of radio-astronomical equipment. His main areas of research are low noise cryogenic amplifiers and mixers, system integration of optical, cryogenic and mechanical components, and research on cryogenic techniques for laboratory applications.

Per-Simon Kildal (M'82-SM'84-F'95) has been a Professor at Chalmers University of Technology, Gothenburg, Sweden since 1989. He has authored an antenna textbook, and more than 100 journal articles and letters in IEEE or IET journals. He has designed two very large antennas, including the Gregorian dual-reflector feed of the Arecibo radiotelescope. He has invented several reflector antenna feeds, the latest being the so-called Eleven antenna. He is the originator of the concept of soft and hard surfaces, recently resulting in the gap waveguide, a new low-loss metamaterials-based transmission line advantageous mainly above 30 GHz. His research group has pioneered the reverberation chamber into an accurate measurement tool for antennas and wireless terminals subject to Rayleigh fading.

Prof. Kildal received two best paper awards for articles published in the IEEE TRANSACTIONS ON ANTENNAS AND PROPAGATION, and he is the recipient of the 2011 Distinguished Achievements Award of the IEEE Antennas and Propagation Society.

Benjamin Klein received the BSc and M.Sc. degrees in Electrical Engineering from the University of Witwatersrand (2003), Johannesburg, South Africa, in 2003 and 2008, respectively. He is currently working on a PhD in a collaboration with HartRAO, Chalmers and the Onsala Observatory. This research is supported by the Swedish Research Council (SDA) and the South African Research Foundation (NRF). He has a wide interest in RF work, and is currently focused on Radio Astronomical receiver noise models, specifically for SKA and VLBI2010.

Yogesh Karandikar was born in 1982 in India. He received the B.E. degree in Electronics and Telecommunication from University of Mumbai in 2004. During 2005, he was with National Center for Radio Astrophysics, TIFR, India. He received his M.Sc. degree in Radio and Space Science in 2007 and Swedish Licentiate degree in 2009 Chalmers University of Technology. He is currently pursuing his PhD at Microwave Electronics Laboratory, Dept. Microtechnology and Nanoscience, at Chalmers. His research interests are broadband feeds for reflector antennas, satellite communication, radio astronomy instrumentation as well as antenna-active devices integration for THz applications.

Leif Helldner is employed as Technician in Operations and Development lab at Onsala Space Observatory since 1989. For more than twenty years he has been working with the development, tests and maintenance of front-end and back-end electronics for radio astronomy. He has excellent experience in the design and tests of RF, IF, automatization and digital electronics, mechanical and cryogenic systems for radio astronomy. He have been in involved in developing hardware systems for the SEST, APEX, ALMA and the Onsala telescopes and radiometers. His interest are mechanical and cryogenic design, and international VLBI and LOFAR technical activities.

Niklas Wadefalk is with the Chalmers University of Technology, Department of Microtechnology and Nanoscience - MC2, SE-412 96 Gothenburg, Sweden.

Christopher J. Beaudoin was born in Peterboro, NH, on October 21, 1977. He received the D.ENG degree in electrical engineering from the University of Massachusetts Lowell (UML) in 2006 for research in physical scale modeling of UHF radar signatures. At the UML Submillimeter Wave Technology Laboratory, he was employed as a senior electrical engineer and conducted research in airborne/ground-based synthetic aperture radar (SAR), designed/constructed compact radar range instrumentation, and developed SAR signal processing algorithms for scale model acquisition of full scale radar signatures. As a natural extension of his radar studies, he also conducted research in computational electromagnetic scattering and analyses in support of the laboratories' signature solution responsibilities. In 2008, Dr. Beaudoin joined the research staff at the MIT Haystack Observatory as a research engineer. In this role, he is a member of the team developing NASA's next generation microwave system for the geodetic Very Long Baseline Interferometry (VLBI) program. This project will reduce the uncertainty in network telescope positions to 1 millimeter on global scales. His contributions to this effort include the design of an ultra low noise (50 Kelvin)/broadband (2-14 GHz) cryogenic front-end, electromagnetic analysis for radio telescope RFI mitigation, development of signal processing algorithms for geodetic delay extraction, and the innovation of monitor/control infrastructure for the NASA geodetic VLBI radio telescope network.